Testing Gravity using the Environmental Dependence of Dark Matter Halos

Gong-Bo Zhao,[1] Baojiu Li,[2,3] and Kazuya Koyama[1]

[1] *Institute of Cosmology & Gravitation, University of Portsmouth, Dennis Sciama Building, Portsmouth, PO1 3FX, UK*

[2] *DAMTP, Centre for Mathematical Sciences, University of Cambridge, Wilberforce Road, Cambridge CB3 0WA, UK*

[3] *Kavli Institute for Cosmology Cambridge, Madingley Road, Cambridge CB3 0HA, UK*

In this *Letter*, we investigate the environmental dependence of dark matter halos in theories which attempt to explain the accelerated expansion of the Universe by modifying general relativity (GR). Using high-resolution N-body simulations in $f(R)$ gravity models which recover GR in dense environments by virtue of the chameleon mechanism, we find a significant difference, which depends on the environments, between the lensing and dynamical masses of dark matter halos. This environmental dependence of the halo properties can be used as a smoking gun to test GR observationally.

PACS numbers: 95.30.Sf, 04.50.Kd, 95.36.+x, 98.80.Jk

One of the biggest challenges in cosmology is to explain the recently observed accelerated expansion of the universe. The acceleration might originate from either "dark energy" within the framework of GR, or from a large-scale modification to GR without introducing new matter species. It could be difficult to distinguish between these two scenarios by merely measuring the expansion rate of the Universe, and one has to study the growth of structure formation in the Universe to break the degeneracy. On large scales, it is possible to perform model independent tests of GR by combining various cosmological observations [1–3], but information on linear scales is limited due to theoretical degeneracies as well as statistical and systematic uncertainties in observations.

There is ample information available about cluster-scale structure formation, but it is difficult to predict the observables on non-linear scales in modified gravity (MG) models. If GR is modified on large scales, there may appear in gravity new scalar degree of freedoms, (dubbed *scalaron*), modifying GR even on cluster scales. In order to evade the stringent constraints on deviations from GR in the solar system, we need a mechanism to recover GR on small scales by screening this scalar mode. In such a mechanism, *e.g.* the chameleon mechanism in $f(R)$ gravity [4, 5], the mass of this scalar mode depends on the local density of matter, becoming heavier in denser environments and thereby suppressing the scalar interaction. This environmental dependence can provide us with a smoking gun for alternative theories to GR [6, 7].

In this *Letter* we investigate and quantify for the first time the environmental dependence of the difference between lensing and dynamical masses for dark matter halos. Our analysis is based on our high-resolution N-body simulations for the $f(R)$ gravity model [8], where the Einstein-Hilbert action in GR is extended to be a general function of the Ricci scalar [9].

In the Newtonian gauge in a general perturbed Friedmann-Roberston-Walker universe, the line element can be written as $\mathrm{d}s^2 = a^2(\eta)[(1+2\Phi)\mathrm{d}\eta^2 - (1-2\Psi)\mathrm{d}\vec{x}^2]$ where η is the conformal time, $a(\eta)$ is the scale factor, Φ and Ψ are the gravitational potential and the spatial curvature perturbation respectively. The Poisson equation reads

$$\nabla^2\Phi = 4\pi G a^2 \delta\rho_{\rm eff}, \tag{1}$$

where G is Newton's constant, and $\delta\rho_{\rm eff}$ is the perturbed total effective energy density, which contains contributions from matter and modifications to the Einstein tensor due to MG. The dynamical mass $M_D(r)$ of a halo is defined as the mass contained within a radius r, inferred from the gravitational potential felt by a test particle at r. It is given by $M_D \equiv \int a^2\delta\rho_{\rm eff}dV$, in which the integral is over the extension of the body. Under the assumption of spherical symmetry, the Poisson equation can be integrated once to give

$$M_D(r) \propto r^2 d\Phi(r)/dr. \tag{2}$$

To measure M_D from our N-body simulation we use the force acting on particles to infer the force acting on each halo as a function of the halo radius and M_D can be obtained using Eq. (2). Observationally, M_D can be estimated from measurements such as velocity dispersions of galaxies. In $f(R)$ gravity M_D includes the contribution from the scalaron, which mediates the finite-ranged fifth force within the Compton wavelength. The mass of the scalaron depends on the local density of matter, resulting in the environmentally-dependent modifications to M_D.

On the other hand, the lensing mass is determined by the lensing potential $\Phi_+ \equiv (\Phi+\Psi)/2$. In $f(R)$ gravity for example, Φ_+ satisfies $\nabla^2\Phi_+ = 4\pi G a^2\delta\rho_{\rm M}$, where $\delta\rho_M$ is the matter density fluctuation if we assume that the background cosmology is close to that for ΛCDM. This is the same equation as in GR, since the scalar mode does not couple to photons and it does not modify light propagation [12]. The lensing mass is defined as $M_L \equiv \int a^2\delta\rho_{\rm M}dV$, and is the actual measured halo mass in our simulations. Thus we will use M_L to represent the halo mass throughout. For a spherically symmetric body we have

$$M_L(r) \propto r^2 d\Phi_+(r)/dr. \tag{3}$$

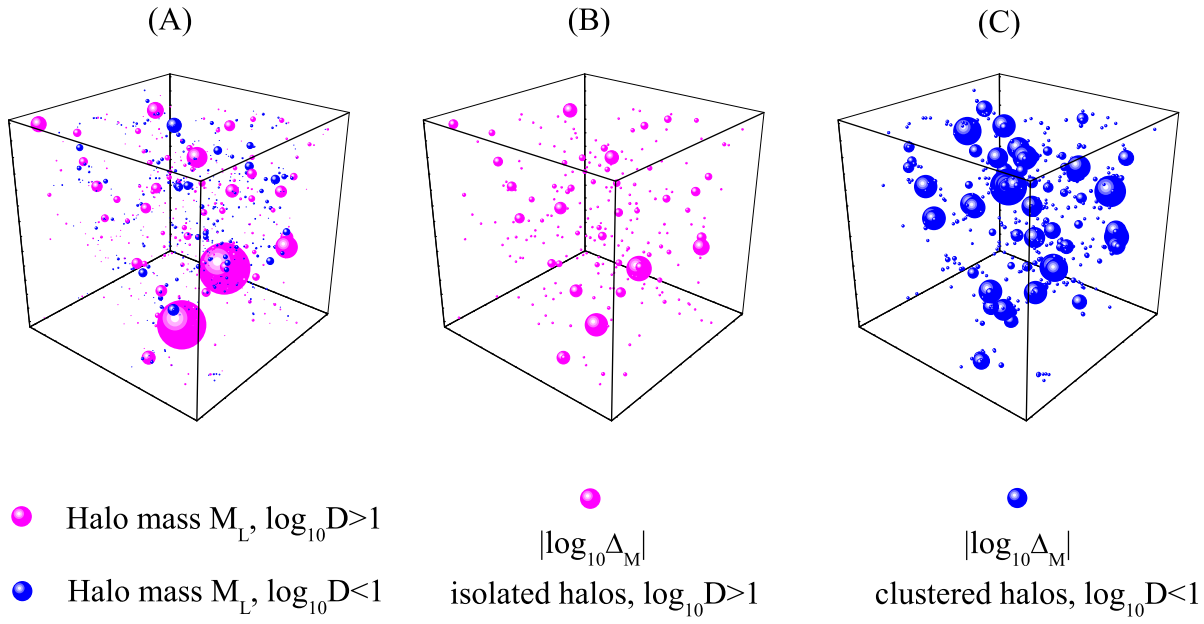

FIG. 1. The illustration of the three-dimensional distributions of the halos (panel A) and the mass difference Δ_M for each halo (B,C) for the $|f_{R0}| = 10^{-6}$ model. The sizes of the bubbles are proportional to the halo mass M_L in (A), and $|\log_{10}\Delta_M|$ in (B,C). In all the panels, the pink and blue bubbles illustrate the isolated halos, and the halos living in the dense environment respectively. See Eq. (5) for the definition of D, which quantifies the environment.

The lensing mass and the dynamical mass are the same in GR, but they can be significantly different in MG scenarios. To quantify the difference, we calculate the relative difference Δ_M between M_L and M_D for each halo, $\Delta_M \equiv M_D/M_L - 1$. Similar quantity, $\mathcal{g} = \Delta_M + 1$, was introduced in Ref. [11]. Combining Eqs (2) and (3), we can rewrite Δ_M as,

$$\Delta_M(r) = \frac{d\Phi(r)/dr}{d\Phi_+(r)/dr} - 1, \tag{4}$$

In GR $\Delta_M(r) = 0$, while in MG models $\Delta_M(r)$ varies depending on the local density.

We have chosen $f(R)$ gravity as a working example to investigate how $\Delta_M(r)$ correlates with both the halo mass and the environment, and propose a new method to test GR based on this correlation. For the analysis we shall use the high-resolution N-body simulation catalogue [8] for a $f(R)$ gravity model, $f(R) = \alpha R/(\beta R + \gamma)$ [10] where $\alpha = -m^2 c_1, \beta = c_2, \gamma = -m^2, m^2 = H_0^2\Omega_{\rm M}$ and c_1, c_2 are free parameters. The expansion rate of the universe in this $f(R)$ model is determined by c_1/c_2, and the structure formation depends on $|f_{R0}|$, which is the value of $|df/dR|$ at $z = 0$, and is proportional to c_1/c_2^2. We tune c_1/c_2 to obtain the same expansion history as that in a ΛCDM model, and choose values for $|f_{R0}|$ so that those models cannot be ruled out by current solar system tests. To satisfy these requirements, we set $c_1/c_2 = 6\Omega_\Lambda/\Omega_{\rm M}$ and simulate three models with

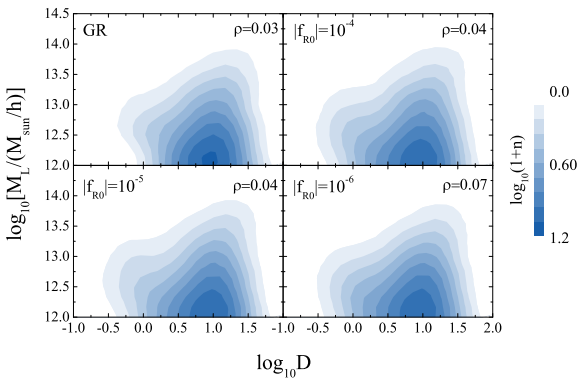

FIG. 2. The contour plots between halo mass M_L and D for $f(R)$ and GR models on a log-log scale. The shaded colour stands for the number density rescaled by the average number density of halos in each pixel on the M_L-D plane.

$|f_{R0}| = 10^{-4}, 10^{-5}, 10^{-6}$.

In $f(R)$ gravity, the effective matter density $\delta\rho_{\rm eff}$ in Eq (1) is given by $\delta\rho_{\rm eff} = \frac{4}{3}\delta\rho_{\rm M} + \frac{1}{24\pi G}\delta R(f_R)$ where δR is the perturbation of the Ricci scalar $\delta R(f_R) = -8\pi G\delta\rho_{\rm M} - \frac{3\nabla^2\delta f_R}{a^2}$ and δf_R is the fluctuation of $f_R \equiv df/dR$. We can see that when the scalar mode vanishes, *i.e.* $\delta f_R = 0$, we recover the GR relation between curvature and matter, $\delta R = -8\pi G\delta\rho_{\rm M}$ and $\Delta_M = 0$. This happens in the dense region where the chameleon has

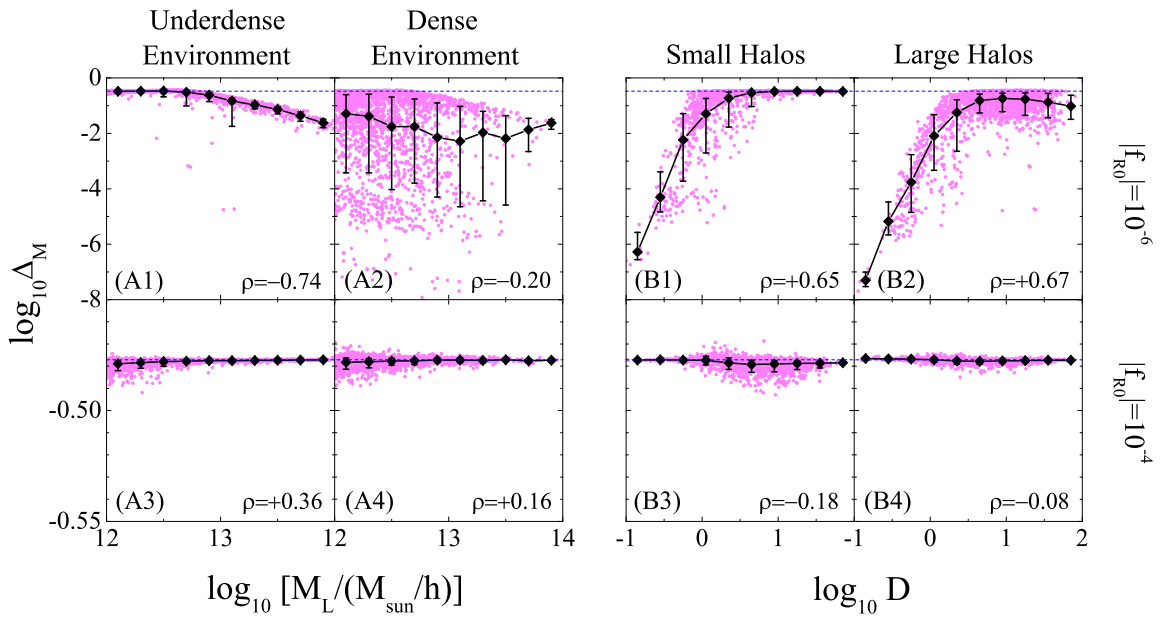

FIG. 3. $\Delta_M(r_{340})$ as a function of halo mass (panels $A1$-$A4$) and D ($B1$-$B4$) for our $f(R)$ models on a log-log scale. Each magenta dot represents one halo in each case, and the black solid line and the error bars show the mean value of $\Delta_M(r_{340})$ and the 1-σ error bars respectively. The correlation coefficient ρ is shown in all cases.

an effect, but in the underdense region where δR can be ignored, $\delta\rho_{\rm eff} = \frac{4}{3}\delta\rho_{\rm M}$ so $\Delta_M = 1/3$. One expects a strong correlation between Δ_M and M_L since halos with large M_L should be 'screened' against the modified gravity influence, and GR be locally restored. This has been confirmed by the previous analysis [8, 11].

The mass threshold for the screening can be estimated theoretically [11]. Interestingly, we find that the small halos with masses below the screening mass threshold can also be well screened if they live in dense environments. This effect is shown visually in Fig. 1. In panel (A) we show the 3-D map of the halo distribution in the $f(R)$ model with $|f_{R0}| = 10^{-6}$ where the size of the bubbles is proportional to M_L, while in panels (B, C) the bubble size is proportional to $|\log_{10}\Delta_M|$. In other words, a larger bubble means a more massive halo in (A), while it means a better screened halo, in which GR is better restored, in (B, C). In all the panels, the pink and blue bubbles illustrate the isolated halos ($\log_{10}D > 1$), and the halos living in the dense environment ($\log_{10}D < 1$) respectively, and these two subsets of halos are complimentary (See Eq. (5) for the definition of D, which quantifies the environment). Panels A and B look almost the same in pattern, meaning that more massive halos are better screened, and the halo mass is the only factor affecting the screening. This is natural since the environmental effect is removed in panel B by design. On the other hand, in panel C, halos living in dense environments are shown, and the environmental effect is the dominating factor for the screening, so that halos with mass below the screening mass threshold can also be efficiently screened. The difference between the panels (A, C) indicates a clear environmental dependence of Δ_M – small halos can be well screened by their neighbouring halos.

This implies that Δ_M correlates with not only M_L, but also the environment. The environment effect was also noticed by Schmidt [11]. In this *Letter*, we shall quantify this effect for the first time. The environmental dependence of Δ_M provides valuable information for testing GR, which compliments the information of the mass-dependence of Δ_M. The amount of information can be maximised if the estimates of the halo mass and environment are uncorrelated.

The 'environment' can be defined such that it suits the physical set-up of the problem, facilitates ease of observations, or both [13]. For our purpose, we need an environment indicator which can represent the local density well, but with least correlation with M_L. Such a quantity was found in Ref. [13],

$$D_{N,f} \equiv \frac{d_{N,M_{\rm NB}/M_L \geqslant f}}{r_{\rm NB}}, \qquad (5)$$

which is defined for a halo with mass M_L as the distance d to the Nth nearest neighbouring halo whose mass is at least f times as large as that of the halo under consideration, rescaled by the virialised radius $r_{\rm NB}$ of that neighbouring halo. Clearly, a large value of $D_{N,f}$ indicates a scarcity of nearby halos, meaning that the considered halo lives in a low-density environment. It is found that in GR, $D_{1,1}$ is almost uncorrelated with the halo mass, and represents the local density well [13].

To test the mass-independence of $D_{1,1}$ in the context of modified gravity, we select the resolved halos from our high-resolution $f(R)$ and GR simulations with boxsize $B = 64$ Mpc$/h$ [8]. In our simulations, the halo mass is measured using $M_L \equiv 4\pi \times N\rho_{\rm crit} r_N^3/3$ where r_N is the radius when the density reaches N times of the critical density of the Universe $\rho_{\rm crit}$, and we choose $N = 340$ [8]. To be conservative, we only select the well-resolved halos from our simulations, *i.e.* halos more massive than $10^{12}h^{-1}M_\odot$. In Fig. 2, we show the contour plots between M_L and D, (we will use D to represent $D_{1,1}$ hereafter for brevity), for three $f(R)$ models in comparison with the ΛCDM model simulated using the same initial conditions. The darkness of the shaded colour quantifies the number density of the halos in each pixel on the M_L-D plane. We follow Ref. [13] to use the Spearman's rank correlation coefficient ρ, which is the correlation coefficient between the ranked variables and varies from -1 to 1, to quantify the correlation between M_L and D. As we can see, they are almost uncorrelated in all cases since the absolute value of the correlation coefficient ρ is much less than unity. This means that the information of the Δ_M-D relation is highly complimentary to that of the Δ_M-M_L relation, which provides us with a new means of testing gravity observationally.

Fig. 3 shows $\Delta_M(r_{340})$ as functions of M_L and D for two $f(R)$ models. To further disentangle the residual correlation between M_L and D, we divide the samples into three subsamples in both cases. In the A panels the halos are divided according to their ordered D values. Halos with D values in the top third of the group ($\log_{10}D \gtrsim 1$) are classified as halos in an 'Underdense Environment' ($A1, A3$), while those with D values in the lowest third ($\log_{10}D \in [-1, 0.65]$) are viewed as halos in an 'Overdense Environment' ($A2, A4$). In the B panels, the halos are separated according to their mass, namely, the halos whose mass is in the top third ($M_L \gtrsim 10^{12.7}M_\odot/h$) are called 'Large Halos' ($B2, B4$), and the third with smallest mass ($M_L \in [10^{12}, 10^{12.3}]M_\odot/h$) are labeled as 'Small Halos' ($B1, B3$). The horizontal blue dashed line shows $\Delta_M(r_{340}) = 1/3$, which is the threshold of Δ_M in $f(R)$ gravity.

As can be seen from Fig. 3, for the $|f_{R0}| = 10^{-6}$ model, $\Delta_M(r_{340})$ decreases when M_L increases, as expected. Note that this anti-correlation is stronger ($\rho = -0.74$) in the underdense regions (panel $A1$), as the environmental effect can be safely ignored in these cases, and $\Delta_M(r_{340})$ is mainly determined by M_L. In the overdense environment ($A2$ for the $|f_{R0}| = 10^{-6}$ case) for the halos with D values in the lowest third, the effect of external environment becomes important – many halos less massive than $10^{12.3}M_\odot/h$ get screened thanks to the boundary conditions set by neighbouring halos. An interesting observation is that some small halos are better screened than the big ones in this case. This is because many small halos reside in overdense environments, surrounded by many neighbouring halos or inside very big halos, while large halos are more likely to be isolated so that their screening is mainly determined by their mass. For the $|f_{R0}| = 10^{-4}$ model, the halos are very weakly screened in all cases, and $\Delta_M(r_{340})$ is close to 1/3, which is the maximum relative mass difference in $f(R)$ gravity. The $|f_{R0}| = 10^{-5}$ case is somewhere in between, and is not shown here.

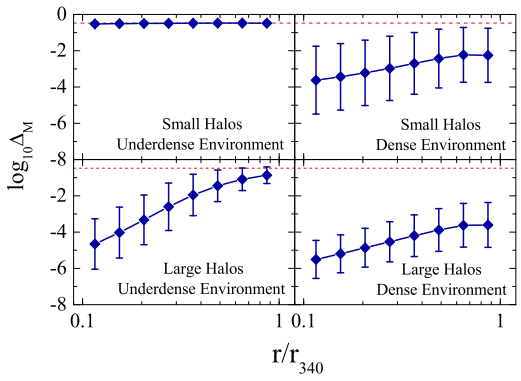

FIG. 4. The profile of $\log_{10}\Delta_M$ as a function of the rescaled halo radius r/r_{340} for the $|f_{R0}| = 10^{-6}$ model. We show the profile with $1-\sigma$ error bars for the halos divided into four categories as illustrated in the legend. The red dashed line shows $\Delta_M(r_{340}) = 1/3$.

The environmental effect can be seen more clearly in the $\Delta_M(r_{340})$-D plot (panels $B1$-$B4$ in Fig. 3). For the $|f_{R0}| = 10^{-6}$ case, we see a strong correlation between the two, and this correlation is largely insensitive to M_L ($\rho \sim 0.7$) in both mass bins. Again, we see that the screening is very efficient in dense regions even for the least massive halos. The correlation between $\Delta_M(r_{340})$ and D for the $|f_{R0}| = 10^{-4}$ case is much weaker, which is because essentially none of the halos are screened by either their own masses or the environment.

We show the profile of the mass difference as a function of rescaled radius for the $|f_{R0}| = 10^{-6}$ model in Fig 4. To see the environment effect on the profile, we split the samples according to both the halo mass and D parameter. As we can see, small halos in the underdense region are hardly screened at all, while the halos with similar mass in the dense region are efficiently screened, and the screening effect is stronger in the core of the halos. For large halos, the innermost part is well screened regardless of external environment due to the high matter density there, but the part close to the edge shows a clear environmental dependence, and the difference can be as large as 3 orders of magnitude in Δ_M in different environments. This is because in this region the external environment plays an important role.

The lensing mass and the dynamical mass can be measured using strong lensing and the peculiar velocity dispersion measurements, respectively, and there has been

some effort to test GR by comparing the two observationally [14, 15]. However, the measurements of the absolute values of Δ_M are likely to be contaminated by systematics. Fortunately, the strong environmental dependence of Δ_M due to the scalar mode in modified gravity theories may provide a way to ameliorate this problem. Observationally, one could divide the galaxy samples into different groups using D, and measure the difference of Δ_M among those subsamples. If a Δ_M-D correlation is found, then it can be viewed as a smoking gun of a modified gravity signal, which can be independently tested using the Δ_M-M_L correlation.

In this *Letter*, we focus on the Chameleon mechanism to recover GR on small scales. There are different classes of mechanism to achieve the screening, such as the Vainshtein mechanism [16] and the symmetron mechanism [17]. In the case of the Vainshtein mechanism, it was found that the screening of halos is almost independent of the environment [11]. Thus the method we proposed provides not only a new independent test of GR on fully nonlinear scales but also a way to distinguish between different screening mechanisms. It is extremely interesting to perform this test using the high-quality observational data from the upcoming large-scale structure surveys.

We thank T. Clemson, R. Crittenden, B. Jain, R. Nichol, L. Pogosian, F. Schmidt and A. Silvestri for discussions. GBZ and KK are supported by STFC grant ST/H002774/1. BL is supported by Queens' College and DAMTP of University of Cambridge. KK acknowledges supports from the ERC and the Leverhulme trust.

[1] Y. -S. Song, K. Koyama, JCAP **0901**, 048 (2009).
[2] G. B. Zhao, L. Pogosian, A. Silvestri and J. Zylberberg, Phys. Rev. Lett. **103** (2009) 241301.
[3] B. Jain, J. Khoury, Annals Phys. **325**, 1479-1516 (2010).
[4] J. Khoury and A. Weltman, Phys. Rev. D **69** (2004) 044026.
[5] B. Li and J. D. Barrow, Phys. Rev. D **75** (2007) 084010.
[6] L. Hui, A. Nicolis, C. Stubbs, Phys. Rev. **D80**, 104002 (2009).
[7] B. Jain, [arXiv:1104.0415 [astro-ph.CO]].
[8] G. B. Zhao, B. Li and K. Koyama, Phys. Rev. D **83** (2011) 044007.
[9] T. P. Sotiriou, V. Faraoni, Rev. Mod. Phys. **82** (2010) 451-497; A. De Felice, S. Tsujikawa, Living Rev. Rel. **13** (2010) 3.
[10] W. Hu, I. Sawicki, Phys. Rev. **D76** (2007) 064004.
[11] F. Schmidt, Phys. Rev. D **81** (2010) 103002.
[12] F. Schmidt, M. V. Lima, H. Oyaizu, W. Hu, Phys. Rev. **D79** (2009) 083518.
[13] M. R. Haas, J. Schaye and A. Jeeson-Daniel, arXiv:1103.0547 [astro-ph.CO].
[14] A. S. Bolton, S. Rappaport and S. Burles, Phys. Rev. D **74** (2006) 061501.
[15] T. L. Smith, arXiv:0907.4829 [astro-ph.CO].
[16] A. I. Vainshtein, Phys. Lett. **B39**, 393-394 (1972).
[17] K. Hinterbichler, J. Khoury, Phys. Rev. Lett. **104**, 231301 (2010).